

Quantification of CO_2 generation in sedimentary basins through Carbonate/Clays Reactions
with uncertain thermodynamic parameters

by, G. Ceriotti^a, G.M. Porta^a, C. Geloni^b and M. Dalla Rosa^b, A. Guadagnini^{a,c}

^aDepartment of Civil and Environmental Engineering, Politecnico di Milano, Piazza L. Da
Vinci 32, 20133 Milano, Italy

^bEni S.p.A.-Upstream and Technical Services, via Emilia, 1 20097 San Donato Milanese
(MI) Italy

^cDepartment of Hydrology and Atmospheric Sciences, University of Arizona, Tucson, AZ
85721, USA

Corresponding author: Giulia Ceriotti, Department of Civil and Environmental Engineering,
Politecnico di Milano, Piazza L. Da Vinci 32, 20133 Milano, Italy, giulia.ceriotti@polimi.it, phone
0039 2399 6257.

Abstract

We develop a methodological framework and mathematical formulation which yields estimates of the uncertainty associated with the amounts of CO_2 generated by carbonate-clays reactions (CCR) in large-scale subsurface systems to assist characterization of the main features of this geochemical process. Our approach couples a one-dimensional compaction model, providing the dynamics of the evolution of porosity, temperature and pressure along the vertical direction, with a chemical model able to quantify the partial pressure of CO_2 resulting from minerals and pore water interaction. The modeling framework we propose allows (i) estimating the depth at which the source of gases is located and (ii) quantifying the amount of CO_2 generated, based on the mineralogy of the sediments involved in the basin formation process. A distinctive objective of the study is the quantification of the way the uncertainty affecting chemical equilibrium constants propagates to model outputs, i.e., the flux of CO_2 . These parameters are considered as key sources of uncertainty in our modeling approach because temperature and pressure distributions associated with deep burial depths typically fall outside the range of validity of commonly employed geochemical databases and typically used geochemical software. We also analyze the impact of the relative abundancy of primary phases in the sediments on the activation of CCR processes. As a test bed, we consider a computational study where pressure and temperature conditions are representative of those observed in real sedimentary formation. Our results are conducive to the probabilistic assessment of (i) the characteristic pressure and temperature at which CCR leads to generation of CO_2 in sedimentary systems, (ii) the order of magnitude of the CO_2 generation rate that can be associated with CCR processes.

Introduction

Natural accumulations of CO_2 are commonly observed in sedimentary basins. The carbon dioxide occurs as a gaseous phase with proportions ranging from 5% to 100% of the total gas phase volume. These CO_2 accumulations are exploited in several sectors, including, for example, the food industry (e.g., Broadhead et al., 2009) or within the context of Enhanced Oil Recovery (EOR; e.g., Allis et al., 2001 and references therein) operations. They are also investigated as natural analogs for improving our understanding and design of subsurface CO_2 storage protocols/technologies and for the assessment of the ensuing environmental risks associated with diverse migration pathways connecting sources with receptors (e.g., Metz et al., 2005). Accumulation of CO_2 in sedimentary basins can lead to dilution of valuable hydrocarbon gas mixtures (e.g., methane and propane), thus reducing energy storage in a reservoir and resulting in an increased production cost (Imbus et al., 1998).

Various authors indicate diverse organic and/or inorganic processes as possible causes of natural CO_2 accumulation (e.g., Higgs et al., 2013; Hutcheon and Abercrombie, 1990; Clayton et al., 1990; van Berk et al., 2013; Smith and Ehrenberg, 1989; Chiodini et al., 2007; Ballentine et al., 2001; Cooper et al. 1997; Dubacq et al., 2012; Fischer et al. 2006; Houtcheon et al., 1980; Imbus et al, 1998; Cathles and Schoell, 2007; Kotarba and Nagao, 2008; Li et al, 2008; Mayo and Muller. 1997; Wycherley et al. 1999; Cai et al. 2001; Farmer, 1965; Goldsmith 1980 Arnórsson, 1986, Chiodini et al., 2000; Fischer et al., 2006). Among these sets of processes, in this study we focus on CO_2 generation in sedimentary formations through the Carbonate/Clay Reaction (CCR) mechanism. The role of CCR as a possible relevant CO_2 generating mechanism in sedimentary systems is originally suggested by Hutcheon and Abercrombie (1990), Hutcheon et al. (1980), Hutcheon et al. (1990), Hutcheon et al. (1993). The feasibility of CCR occurrence in a sedimentary environment is supported by a significant amount of studies (e.g., Coudrain-Ribstein and Gouze, 1993, Coudrain-Ribstein et al., 1998, Cathles and Schoell, 2007; Giggenbach, 1980; Smith and Ehrenberg, 1989; Chiodini et al.,

2007; Xu and Pruess, 2001; van Berk et al., 2009). These works document a series of field data about CO_2 partial pressure and/or pore-water chemical compositions sampled in real sedimentary basins and/or computed through geochemical speciation models which are compatible with the CCR mechanism. Cathles and Schoell (2007) propose a clear and schematic conceptual model of CO_2 generation through CCR and provide a mathematical formulation relying on a chemical equilibrium model for the identification of the environmental conditions (temperature and pressure) at which CO_2 may be generated as a separate gas phase. These authors illustrate the use of their model through an exemplary setting assuming a time-invariant linear relationship between temperature and pressure, along the lines of Smith and Ehrenberg (1989). The results of this study suggest that CCR may become a relevant process for gaseous CO_2 generation at a temperature of about 330 °C. Even as the results of the illustrative example of Cathles and Schoell (2007) are not directly transferable to a real sedimentary basin setting (where temperature and pressure vary with time according to a higher complexity pattern), they clearly suggests that the CO_2 gas generation associated with CCR is expected to occur at very high temperatures and pressures.

Uncertainties associated with thermodynamic parameters characterizing CCR are virtually ubiquitous. This is the consequence of a variety of factors (including, e.g., intrinsic natural variability of mineral compositions, non-ideal behavior of multiphase solutions, paucity and/or inaccuracy of available experimental data) and constitutes a critical challenge for the robust characterization of geochemical processes taking place at high temperature and pressure which are typically observed in deep sedimentary formations.

In this context, the major objective of our study is to propose a general framework within which we develop a modeling approach which incorporates the uncertainty associated with the thermodynamic parameters characterizing the CCR mechanism to yield a quantitative estimation of the amount of CO_2 released from CCR in sedimentary formations. Our approach is grounded on two coupled components: (i) a compaction model, simulating the burial history of a sedimentary basin; and (ii) a geochemical model which quantifies the amount of generated CO_2 (as a dissolved or

separate gaseous/supercritical phase) on the basis of thermodynamic equilibrium concepts. For the purpose of demonstrating our approach, we consider the one-dimensional compaction model presented by Formaggia et al. (2013), Porta et al. (2014) and Colombo et al. (2016), other numerical models (eventually characterized by an increased degree of complexity) being fully compatible with our methodological framework. Quantification of CO_2 in aqueous and gaseous phase in surface environments or shallow subsurface systems is generally tackled through a hydro-geochemical speciation software (e.g., Phreeqc, Parkhurst and Appelo, 2013). Available databases supporting these software are typically considered as reliable within a range of temperatures lower than 300 °C. Settings of the kind investigated in this study are characterized by temperatures larger than 300 °C and pressure values significantly larger than those typically found in shallow aquifer systems. Hence, we employ here an *ad-hoc* geochemical model which is consistent with the formulations proposed by Giggenbach (1981), Coudrain-Ribstein et al. (1998) and Cathles and Schoell (2007) and can be applied in the presence of temperature/pressure conditions taking place in deep sedimentary formations.

We highlight that a major element of novelty of our work is the analysis of the way uncertainties associated with the thermodynamic parameters employed to characterize the CCR mechanism, i.e., the mineral solubility and phase equilibrium constants, propagate to the final model outputs. These parameters are viewed as random model inputs characterized by a given probability density function (*pdf*). As a consequence, all outputs are considered in a probabilistic framework. A variety of additional sources of model and parametric uncertainty (Neuman, 2003) may affect the outputs of the proposed modeling approach. These include, e.g., the salinity of the brine and the feedback with other geochemical processes which may take place in sedimentary systems. In this work we focus on the characterization of parametric uncertainty related to thermodynamic equilibrium constants, because these parameters are not firmly constrained at the pressure and temperature conditions of interest. To the best of our knowledge, an assessment of this kind is still lacking in the context of basin scale modeling of CCR processes.

Key target quantities that we consider as model outputs are the amount of CO_2 produced in the system and its temporal dynamics resulting from the compaction processes of the sediment evolving along geologic time scales. Results stemming from our approach include an explicit quantification of the depth at which the source of gaseous CO_2 is located and of the impact of the relative abundance of primary phases affecting the generation of CO_2 . As a first test bed to illustrate our methodology, we implement the conceptual and numerical model proposed on a realistic sedimentary basin setting in terms of temperature-pressure-porosity, upon considering multiple scenarios in terms of relative abundance of CCR primary phases in the mineralogical assemblage. We base this study on a streamlined conceptual and numerical model of the system to allow (i) focusing on the stochastic analysis of selected uncertain quantities and (ii) comparing our results against available literature data. As such, we consider uncertainty to be embedded in the effects of the temperature on the thermodynamic constants regulating the equilibrium between CO_2 - water - mineral phases, all of the remaining model features being treated as deterministic (see also Section 3 for a detailed discussion). The methodological framework we propose is then portable to scenarios characterized by an increased level of complexity and in the presence of a variety of sources of uncertainty.

The work is structured as follows: in Section 1 we provide a brief overview of the CCR process; Section 2 illustrates the theoretical framework and modeling workflow as well as the coupled formulation of the geochemical and basin models we employ to quantify the CO_2 generated during the basin evolution; in Section 3 we illustrate the main sources of uncertainty which can arise in our modeling procedure and classify these into modeling and parametric uncertainties; in Section 4 we present the main results obtained by the implementation of the modeling workflow for a basin-scale case study; Section 5 is devoted to a detailed discussion and analysis of the results. We provide conclusions and an overview on future perspectives in Section 6.

1 Overview of CCR processes

Previous works (e.g. Giggenbach, 1980) have shown that the presence of carbonate phases along with clays and/or alumino-silicates in high-temperature geothermal or sedimentary systems acts as a buffer system for the pore-water and might then control the partial pressure of CO_2 . Assuming that the rock-fluid system attains an equilibrium, we can model the interaction between carbonates, alumino-silicates, clays and CO_2 as a single equilibrium reaction. The latter is typically termed Carbonate/Clays Reaction (CCR), following the nomenclature introduced by Hutcheon et al. (1980).

Several authors (Giggenbach, 1978; Giggenbach, 1981; Giggenbach, 1984; Coudrain-Ribstein et al., 1998; Cathles and Schoell, 2007; Hutcheon and Abercrombie, 1990; Hutcheon et al., 1980; Hutcheon et al., 1989; Hutcheon et al., 1993; Zhang et al., 2000; Huang and Longo, 1994; Ueda et al., 2005) suggest a variety of chemical equilibrium relationships to depict the stoichiometry of CCR. Table 1 lists a set of CCRs following the study of Coudrain-Ribstein et al. (1998). These can be generalized through a chemical equilibrium relationship of the kind

$$\alpha_1 M_1 + \dots + \alpha_m M_m = \alpha_{m+1} M_{m+1} + \dots + \alpha_{n+m} M_{n+m} + \alpha_0 CO_{2(g)} \quad (1)$$

where M_k ($k = 1, \dots, n+m$) represents the k^{th} mineral phase involved in the process and α_k are stoichiometric coefficients.

Since the generation of CO_2 is the result of the consumption of the mineral phases of the left hand side of (1), we indicate M_k with $1 \leq k \leq m$ or $m+1 \leq k \leq m+n$ as primary or secondary phases of the system, respectively. Primary phases include a carbonate mineral (which represents the source of CO_2) together with other cations (e.g., Mg^{+2} and Ca^{+2}), and additional clay/alumino-silicate phases. The latter act as source of other ions (e.g., OH^- , Al^{3+} and K^+) when dissolved in water. All reactions listed in Table 1 include dolomite as carbonate mineral. The secondary phases include CO_2 , clay minerals (e.g., chlorite, phlogopite, illite; Bergaya and Lagaly, 2013) and other species (e.g., calcite) which act as sinks for the ions released by the primary phases and represent a more stable mineralogical assemblage at large temperature (e.g., $T > 300$ °C), as compared to primary phases

(Giggenbach, 1981; Hutcheon and Abercrombie, 1990; Smith and Ehrenberg, 1989). Partitioning among primary and secondary phases in the system can be described through the equilibrium constant (K_R). All phases appearing in (1) are in pure liquid or solid phases, CO_2 being the only gaseous phase. The logarithmic transform of K_R is

$$\log K_R = \alpha_0 \log \eta_{CO_2(g)} + \sum_{k=m+1}^{n+m} \alpha_k \log a_{M_k} - \sum_{k=1}^m \alpha_k \log a_{M_k} \quad (2)$$

a_{M_k} and η_{CO_2} respectively representing the activity of species M_k and the CO_2 fugacity. Assuming that the fugacity coefficient of CO_2 is equal to one (Hutcheon, 1990, Chiodini et al., 2007; Cathles and Schoell, 2007; Coudrain-Ribstein et al., 1998) yields

$$\log P_{CO_2} = \log \eta_{CO_2(g)} = \frac{\log K_R}{\alpha_0} \quad (3)$$

P_{CO_2} being the partial pressure of CO_2 either in the gaseous or supercritical phase. Note that, according to our assumption, the numerical values of CO_2 fugacity and partial pressure coincide (Anderson, 2009). We provide additional discussion about the assumption of $\eta_{CO_2} = P_{CO_2}$ in Electronic Annex II. The value of $\log K_R$ (and therefore P_{CO_2}) is a function of the local conditions of pressure and temperature, as discussed in Sections 2.2.

The CCR process can be summarized by the phenomenological scheme illustrated in Fig. 1 and described in the following.

1. Given a sedimentary rock containing carbonates and clays/alumino-silicates, the amount of dissolved CO_2 in the pore water is regulated by the chemical equilibrium among all phases (Fig. 1a). Even as a separate gas phase is not formed, the concept of partial pressure associated with gaseous species can be still preserved if referred to a fictive gas phase hypothetically at equilibrium with the pore water (Coudrain-Ribstein et al., 1998).
2. Pressure and temperature typically increase throughout the burial process. Under these conditions, the sum of the partial pressures associated with gaseous species (CO_2 and possibly

other species including, e.g., $H_2O_{(g)}$, $CH_{4(g)}$) might exceed the fluid environmental pressure.

When this happens, a separate gas phase is generated (Fig.1b). In this work we consider only CO_2 and H_2O as possible gaseous species.

3. When CO_2 (possibly mixed with other gases) is released as a gas phase, the difference between gas and fluid phase densities promotes upward migration of CO_2 . As a consequence of this migration, the equilibrium reaction (1) is shifted towards its right side (Fig. 1c) and the reactions listed in Table 1 can be considered as a quantitative transformation of the reactants (primary phases) into the products (secondary phases), as seen, e.g., in Cathles and Schoell (2007).

Note that supercritical CO_2 is likely to be expected at the pressure and temperature conditions characterizing sedimentary formations. We assume that the conceptual model proposed by Cathles and Schoell (2007) still holds when CO_2 is in supercritical conditions. Supercritical CO_2 is always characterized by lower density when compared to water and buoyancy effects always force the CO_2 -rich separate gas phase to migrate upwards as soon as it is generated (Battistelli et al., 2016; Span and Wagner, 1996; Johnson et al., 1992). For simplicity, we refer in the following to the separate CO_2 -rich phase as gaseous CO_2 .

When the conditions for the generation of a separate gas phase are not attained, CCR leads only to the formation of aqueous CO_2 which remains dissolved in the pore-fluid. Dissolved CO_2 can constitute a significant fraction of the overall CO_2 amount released by CCR and its occurrence can be a relevant aspect to consider when the characterization of flow processes in sedimentary formations is of concern (Coudrain-Ribstein and Gouze, 1993; Chiodini et al., 2000; Farmer, 1965).

2 Modeling workflow

We illustrate here a procedure to compute the time, depths and temperature at which the process described in Fig. 1, i.e. the activation of the gaseous CO_2 source, takes place. The two main constituents of the numerical modeling procedure we propose are:

1. a basin compaction model, providing the temporal dynamics of porosity, temperature, pressure and basin stratigraphy along the vertical direction in the presence of mechanical compaction;
2. a geochemical model which allows computing the partial pressure of CO_2 (P_{CO_2} [Pa]) and the concentration of dissolved CO_2 (C_{CO_2} [mol/L]) as a function of temperature and pressure.

Our modeling strategy focuses on the uncertainty associated with the identification of CO_2 sources and with the quantification of the resulting CO_2 fluxes. Characterization of migration of CO_2 after its generation is beyond the scope of our study. Fig. 2 illustrates the key steps of the workflow, which is subdivided in three blocks: *i*) implementation of the burial model (Block 1), described in Section 2.1; *ii*) computation of the CO_2 pore-water concentration and CO_2 partial pressure (Block 2), illustrated in Section 2.2; and *iii*) estimation of CO_2 generation rate and source location (Block 3), detailed in Section 2.3. All details on the computational steps of the model are reported in the Electronic Annex I where a step-by-step illustration of the procedure is included to assist reproducibility of the model implementation.

2.1 Basin Model

The quantification of the amount of CO_2 generated in sedimentary systems requires the quantification of (*i*) porosity (ϕ), temperature (T), pressure (P) distributions and burial velocity of sediments (V_{SED} , i.e., rate at which the sediments are displaced along the vertical direction) as a function of depth and time; and of (*ii*) the temporal evolution of the stratigraphy. In this study, we obtain these quantities through the one-dimensional compaction model proposed and tested by Formaggia et al. (2013), Porta et al. (2014), and Colombo et al. (2016). Further details related to the burial model implemented in this work can be found in Electronic Annex I. We highlight here that any type of compaction/diagenesis model (e.g., a three-dimensional model) is compatible with the proposed procedure, provided it renders a characterization of the dynamics of temperature, pressure, porosity and sediment burial velocity in the system. In this study, we consider the outputs of the basin model

(e.g., temperature and pressure distributions) as deterministic quantities, consistent with our focus on the quantification of the parametric uncertainty related to the geochemical model. Possible sources of uncertainty affecting the burial model are explicitly discussed in Section 3.

2.1.1 Basin scale case study and compaction setting

We illustrate the applicability of our methodological framework for the quantification of the uncertainty associated with estimates of CO_2 generation at basin scale by focusing on an exemplary system inspired to a realistic compaction setting.

We consider a basin deposition over a period of 135 Ma (Millions of years before present), from time $t = 135$ Ma, to present day (i.e., $t = 0$ Ma). According to our simplified compaction model, we assume the basin to be described as a one-dimensional system along the vertical direction. The paleo-bathymetry is constant and set equal to an elevation of 106 m (the Z -axis is considered to point downwards and the sea level to correspond to $Z = 0$). Carbonate sediments are deposited within the interval ranging from time $t = 135$ Ma and $t = 23$ Ma, leading to the formation of carbonate rock layers. Shale and sandy shale sediments are deposited within the period ranging from $t = 23$ Ma and $t = 0$ Ma, leading to mudrock after compaction. Sediment deposition rate (V_D) at the basin top is imposed as boundary condition. We assume that it varies in time and can be described by a piecewise constant function of time across six time intervals as indicated in Table 2. A given temperature gradient of $32\text{ }^\circ\text{C/km}$ is prescribed at the basement. Each sediment type is characterized by a given thermal conductivity of the solid matrix (K_T), initial porosity (i.e., porosity at sediment deposition time, ϕ_0), and vertical compressibility coefficients (β). We set the parameters K_T , ϕ_0 and β to the values listed in Table 3.

We analyze the two possible scenarios of mineral composition associated with carbonate rock listed in Table 4. We highlight that: (i) Scenario S_{dol} considers dolomite as the only carbonate mineral

present in the rock; (ii) Scenario S_{cal} is characterized by the presence of magnesiatic limestone where calcite is the prevailing carbonate (73% in weight) and the fraction of dolomite is lower than 10.

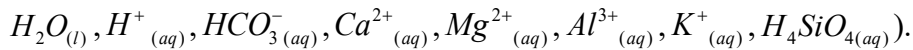
2.2 Geochemical modeling under uncertainty

The main physical quantities which allow quantifying the CO_2 generated by CCR are the partial pressure of the gas phases and the concentration of the CO_2 dissolved in the fluid phase. We obtain these outputs starting from (1)-(3) and relying on the assumption that the activity of the pure solid mineral and liquid phases are set equal to unity (Giggenbach, 1980; Giggenbach, 1984).

The dependence of P_{CO_2} on temperature in (3) is assessed by relying on the thermochemical parameters collected in a thermodynamic database. Among the databases available in the literature (e.g., LLNL, Delany and Lundeen, 1990; Vminteq, Peterson, 1987; SOLMINEQ, Kharaka et al., 1988), we select the Thermoddem database (Blanc et al., 2012) due to its completeness, traceability of data, and proven internal thermodynamic consistence, especially for the aluminum silicate phases (Blanc et al., 2015).

In the remainder of the work, an uncertain (i.e., random) quantity ζ is identified with the notation $\tilde{\zeta}$. Our operational procedure relies on the following steps:

1. A set of basis species is selected coherently to the chosen thermodynamic database (e.g.,



2. A set of stoichiometric coefficients are defined to honor mass and charge balances, i.e.,

$$\begin{cases} \gamma_k = \alpha_k & \text{if } 1 \leq k \leq m \\ \gamma_k = -\alpha_k & \text{if } m+1 \leq k \leq m+n \end{cases} \quad (4)$$

3. A speciation reaction S_k is defined for each M_k phase ($k= 1, \dots, n+m$) involved in reaction (1) to describe speciation in the formation fluid (which we consider as water) of M_k through the basis species selected in step 1. Uncertain chemical equilibrium constants \tilde{K}_{S_k} are quantified to characterize the speciation reaction S_k of phase M_k at temperature T . We do so by employing

the following equation derived from the Maier-Kelley heat capacity definition (Maier and Kelley, 1932; Parkhurst and Appelo, 2013; van Berk et al., 2009)

$$\log \tilde{K}_{Sk} = \tilde{A}_k + \tilde{B}_k T + \frac{\tilde{C}_k}{T} + \tilde{D}_k \log T + \frac{\tilde{E}_k}{T^2} \quad (5)$$

where $(\tilde{A}_k, \tilde{B}_k, \tilde{C}_k, \tilde{D}_k, \tilde{E}_k)$ is a vector of uncertain quantities which are treated as independent random variables/parameters with an assigned probability density function (*pdf*). The characterization of the uncertainty of these parameters is discussed in Section 2.2.1. Note that the (5) allows evaluating the equilibrium constant \tilde{K}_{Sk} as a function of temperature while keeping the pressure of the system at a constant reference value of 1 bar.

4. The equilibrium constant $\log \tilde{K}_{R,T,1}$ associated with reaction (1) is computed as (Coudrain-Ribstein et al., 1998)

$$\log \tilde{K}_{R,T,1} = \sum_{k=1}^n \gamma_k \log \tilde{K}_{Sk} - \alpha_0 \log \tilde{K}_{S,CO2(g)} \quad (6)$$

where $\tilde{K}_{S,CO2(g)}$ is the equilibrium constant associated with the reaction defining the CO_2 (either gaseous or supercritical) in terms of its basis species. Note that $\tilde{K}_{S,CO2(g)}$ is considered to be characterized by a relationship having the same format as (5) and is also considered as random. Subscript 1 appearing in $\log \tilde{K}_{R,T,1}$ indicates that the value of the equilibrium constant evaluated through (6) is associated with the reference pressure of 1 bar.

5. We compute $\tilde{K}_{R,T,P}$ as a modification of $\tilde{K}_{R,T,1}$ to account for the high pressure at which the CCR process occurs according to the procedure proposed by Millero (1982). Further details can be found in Electronic Annex I.
6. CO_2 partial pressure \tilde{P}_{CO2} is evaluated upon replacing $\log K_R$ with $\log \tilde{K}_{R,T,P}$ in (3).

The activity $\tilde{a}_{CO2(aq)}$ of carbon dioxide dissolved in the liquid phase can be estimate by considering the equilibrium as an effective model

$$CO_{2(g)} = CO_{2(aq)} \quad (7).$$

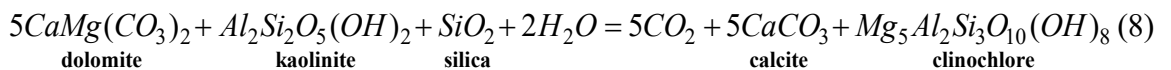
Assuming a unit coefficient activity associated with $[CO_{2(aq)}]$ (see Electronic Annex II for additional details about this assumption), we can directly derive the molar concentration of aqueous CO_2 ($\tilde{C}_{CO_2(aq)}$ [mol/l]) from the CO_2 activity. A description of the detailed steps leading to the quantification of aqueous CO_2 through our computational procedure are included in Electronic Annex I.

Values of the uncertain quantities $\tilde{C}_{CO_2(aq)}$ and \tilde{P}_{CO_2} may be constrained by the effect of limiting reactants, as a consequence of relative abundancy of diverse primary phases. Given a mineral composition, the generation of CO_2 takes place according to the equilibrium relationship (3) until one of the involved primary mineral phases vanishes. We then verify that the computed $\tilde{C}_{CO_2(aq)}$ is compatible with the maximum CO_2 concentration (C_{max}) associated with the complete depletion of the limiting reactant across all primary phases. We set $C_{CO_2(aq)} = C_{max}$ at locations where $C_{CO_2(aq)}$ is larger than C_{max} , and accordingly correct the associated value of P_{CO_2} . In the following we denote as $\tilde{C}_{CO_2(aq)}|_{C_{max}}$ and $\tilde{P}_{CO_2}|_{C_{max}}$ the values of dissolved CO_2 and CO_2 partial pressure conditional to the effect of limiting reactant. Additional computational details related to C_{max} , $\tilde{C}_{CO_2(aq)}|_{C_{max}}$, and $\tilde{P}_{CO_2}|_{C_{max}}$ are included in Electronic Annex I.

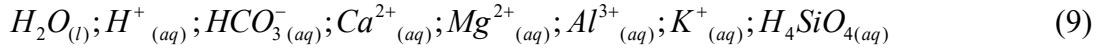
2.2.1 Characterization of uncertain model inputs

Here we illustrate the stochastic characterization of the chemical equilibrium constants. We assess the consistency of the results stemming from the proposed procedure with available data of CO_2 partial pressure in Sections 4.2 and 5.1.

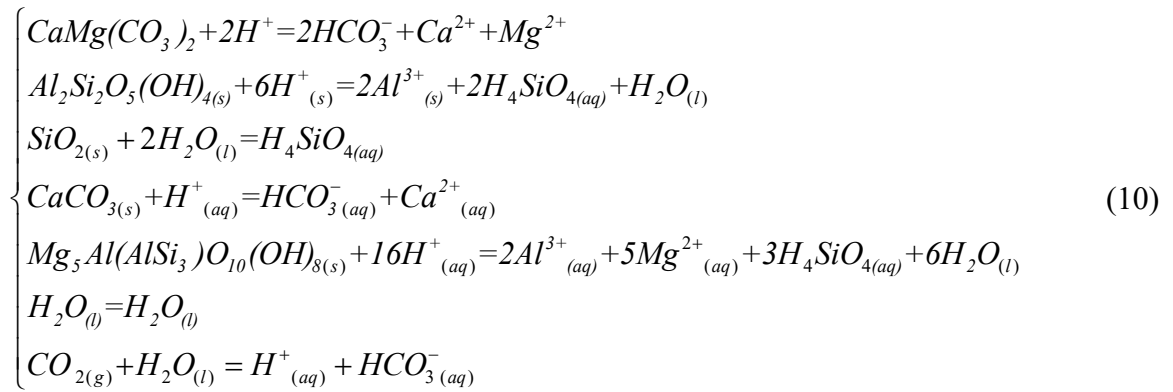
For the purpose of illustration of our uncertainty quantification procedure, hereinafter we focus on the following CCR (see Table 1)



We select this equilibrium reaction among those listed in Table 1 because all of the involved mineral phases are commonly found in sedimentary system (e.g., Hutcheon, 1990; Coudrain-Ribstein and Gouze, 1993) and it is in agreement with the mineralogical assemblage alteration observed in the Kootenay Formation studied by Hutcheon et al. (1980). We follow the procedure outlined in Section 2.2 and start by selecting the following basis species



We then write the following system governing speciation of all liquid and solid phases involved and of the gaseous CO_2



We characterize the equilibrium constants associated with (10) by relying on Thermoddem as a reference database (Blanc et al., 2012). We employ (5) to account for the influence of temperature, where parameters $(\tilde{A}_k, \tilde{B}_k, \tilde{C}_k, \tilde{D}_k, \tilde{E}_k)$ are assumed to be uncertain.

To streamline the uncertainty quantification procedure, we perform a preliminary sensitivity analysis by means of a numerical Monte Carlo procedure. This enables us to single out the contributions of the five parameters appearing in (5) to the variability of \tilde{K}_{S_k} characterizing the reactions S_k presented in (10). In this framework, the five parameters $(\tilde{A}_k, \tilde{B}_k, \tilde{C}_k, \tilde{D}_k, \tilde{E}_k)$ associated with the quantification of each $\log \tilde{K}_{S_k}$ are randomly sampled from uniform distributions centered on the reference value reported in Thermoddem and of width equal to $\pm 20\%$ of such reference value. We compute the first order sensitivity index ($SI_h, h = A, B, C, D, E$) for each parameter, according to

the variance-based method described, e.g., in Sobol (2001), Saltelli et al. (2008), and Razavi and Gupta (2015). These sensitivity indices represent the relative contribution of each uncertain parameter in (5) to the variance of $\log \tilde{K}_{sk}$. These metrics are widely employed in diverse fields (e.g., Saltelli et al., 2008; Formaggia et al., 2013; Porta et al., 2014; Riva et al., 2015) to perform global sensitivity analysis of the output of a model as driven by a set of uncertain (random) model parameters. The results of this analysis reveal that the variability of $\log \tilde{K}_{sk}$ computed through (8) is mainly due to the random variability of parameters \tilde{A}_k and \tilde{D}_k (details not shown). These parameters are always associated with first order sensitivity indices (SI_A and SI_D) larger than 0.43 for $0\text{ }^{\circ}\text{C} \leq T \leq 400\text{ }^{\circ}\text{C}$, SI_B , SI_C and SI_E always being lower than 0.02. On these bases, we set parameters B , C and E to the values listed in Thermoddem and consider \tilde{A}_k and \tilde{D}_k as random input parameters in (5).

We rely on laboratory scale mineral solubility experiments to characterize the uncertainty associated with \tilde{A}_k and \tilde{D}_k . As observed by Blanc et al. (2013), only a few experimental studies reporting values of \tilde{K}_{sk} as a function of temperature are available, particularly with reference to clay minerals. The estimation of the coefficients embedded in Thermoddem is mostly based on thermodynamic calculations, which are associated with an uncertainty level which is difficult to quantify. Here, we employ the mineral solubility data for calcite and kaolinite reported by Plummer and Busenberg (1982) and Blanc et al. (2013). Plummer and Busenberg (1982) provide observations of the calcite speciation constant for a series of temperatures ranging from 0.1 $^{\circ}\text{C}$ to 89.7 $^{\circ}\text{C}$. Blanc et al. (2013) collect a set of solubility experimental data related to kaolinite previously presented by various authors and associated with temperature values ranging between 25 $^{\circ}\text{C}$ and 300 $^{\circ}\text{C}$.

We employ the following procedure to quantify uncertainties associated with \tilde{A}_k and \tilde{D}_k . (with i = kaolinite, calcite) using the solubility experimental data indicated above:

1. We calibrate model (5) against available experimental observations K_{sk}^* upon estimating the parameters \tilde{A}_k and \tilde{D}_k (with k = calcite, kaolinite) through a standard least square criterion.

As indicated above, parameters B_k , C_k , E_k are set to the corresponding values reported in Thermoddem. This procedure yields best estimates (\hat{A}_k, \hat{D}_k) of parameters $(\tilde{A}_k, \tilde{D}_k)$ and the related uncertainty expressed in terms of a 2×2 symmetric covariance matrix $\hat{\Psi}_k$. The results of these calculations are listed in the first two rows of Table 5.

2. We consider that the entries of the uncertain parameter vectors $\tilde{\mathbf{u}}_k = (\tilde{A}_k, \tilde{D}_k)$ can be described through a bivariate Gaussian distribution with mean $\mu(\tilde{\mathbf{u}}) = (\hat{A}_k, \hat{D}_k)$ and covariance matrix $\Psi_k = \hat{\Psi}_k$ (with $k = \text{calcite, kaolinite}$).

No direct references are reported in the Thermoddem database to characterize the uncertainty associated with the equilibrium constants related to the remaining phases included in (8) (dolomite, clinochlore, quartz, $CO_{2(g)}$, $CO_{2(aq)}$). In our illustrative example we resort to the following set of assumptions to characterize uncertainties associated with \tilde{A}_k and \tilde{D}_k (with $k = \text{dolomite, clinochlore, quartz, } CO_{2(g)}, CO_{2(aq)}$):

1. The vector of parameters $\tilde{\mathbf{u}}_k = (\tilde{A}_k, \tilde{D}_k)$ (with $k = \text{dolomite, clinochlore, quartz, } CO_{2(g)}, CO_{2(aq)}$) is associated with a bivariate Gaussian distribution. Here, we assume that the entries of the vector of mean values $\mu(\tilde{\mathbf{u}}_k)$ coincide with the values included in Thermoddem for each phase k (see Table 5).
2. Affine minerals are characterized by the same parametric uncertainty, i.e., we set $\Psi_{\text{dolomite}} = \hat{\Psi}_{\text{calcite}}$ (as dolomite and calcite are both carbonates minerals) and $\Psi_{\text{clinochlore}} = \hat{\Psi}_{\text{kaolinite}}$ (as clinochlore and kaolinite are both clay minerals, Bergaya and Lagaly, 2013).
3. The parameters describing the solubility of quartz and the water transition phase equilibrium are characterized by negligible uncertainty when compared against the uncertainty level of the equilibrium constants discussed above.

4. We set $\Psi_{CO2(g)} = \Psi_{CO2(aq)} = \hat{\Psi}_{kaolinite}$, as $\hat{\Psi}_{kaolinite}$ renders the highest level of uncertainty following estimation of the coefficients of (5) through the experimental data employed (i.e., solubility data of calcite and kaolinite).

Mean values of the parameter distributions are listed in Table 5 together with the associated covariance matrix entries and the set of assumptions illustrated above. Note that these assumptions are not strictly required for the applicability of the proposed methodology and are here considered solely for illustrative purposes. In this sense, measurements on mineral solubility or equilibrium constants can readily be integrated in the proposed workflow when available.

2.3 Quantitative assessment of CO_2 generation and CCR mechanism activation at basin scale

The basin compaction and geochemical models illustrated in Sections 2.1 and 2.2 allow assessing the desired dynamics of the CCR mechanism and quantifying the amount of CO_2 generated (as gaseous or dissolved species) during the diagenetic process.

Generation of a separate gas phase at a location Z and time t takes place when

$$\tilde{R}(Z,t) = \frac{\tilde{P}_{gas}(Z,t)}{P(Z,t)} = \frac{\tilde{P}_{CO2}(Z,t) + P_{H2O}(Z,t)}{P(Z,t)} \geq 1 \quad (11)$$

where $P(Z,t)$ and $\tilde{P}_{gas}(Z,t)$ respectively are the fluid pressure and the partial pressure of the gas phase. Note that $P(Z,t)$ is rendered by the basin compaction model of choice (see Section 2.1) while \tilde{P}_{CO2} is evaluated through the procedure illustrated in Section 2.2. The computation of partial pressure of water vapor, $P_{H2O}(Z,t)$, is detailed in Electronic Annex I. According to criterion (11), the space-time locations at which the generation of gaseous CO_2 may take place can be identified through the local values of the ratio \tilde{R} . For a given time level t , the activation of the mechanism is assigned to the location

$$\tilde{Z}_{act}(t) = \begin{cases} \emptyset & \text{if } \tilde{R} < 1 \text{ for all } Z \in \Omega_Z \\ \min \{ Z \in \Omega_Z \mid \tilde{R}(Z, t) \geq 1, m_{CO_2} > 0 \} & \text{if } \exists Z \in \Omega_Z \mid \tilde{R}(Z, t) \geq 1 \end{cases} \quad (12)$$

i.e., the location of the CO_2 source at time t , $\tilde{Z}_{act}(t)$, is assumed to correspond to the shallowest depth at which $\tilde{R} \geq 1$, given that the mineral composition is compatible with CCR. Note that $\tilde{Z}_{act}(t)$ is a function of time because of the temporal variability of vertical profiles of temperature and pressure. Definition (12) is consistent with the assumption that CO_2 migrates instantaneously upwards when a gas phase is formed (see Fig. 1). Under such conditions, the primary phases of the equilibrium reaction (1) are progressively consumed because one of the secondary phases (CO_2) is continuously driven away. This behavior is observed until the limiting reactant in (1) vanishes. We assume that the complete consumption of at least one primary phase takes place on a time scale that is considerably smaller than the one associated with the basin evolution. Therefore, the burial velocity of the sediment, $V_{SED}(\tilde{Z}_{act}, t)$, is a limiting factor for the generation of CO_2 as a gas phase through a CCR mechanism. Under this assumption, we can then evaluate the rate of CO_2 generation as

$$\tilde{F}_{CO_2}(t) = m_{CO_2} \cdot V_{SED}(\tilde{Z}_{act}, t) \cdot [1 - \phi(\tilde{Z}_{act}, t)] \cdot L \cdot \rho \quad (13)$$

Here, \tilde{F}_{CO_2} [kg/Ma] is the CO_2 mass generation rate; L [m²] is the planar cross sectional area of the basin/reservoir; and m_{CO_2} [-] is maximum amount of mass of CO_2 released by unity mass of sediment (see Electronic Annex I for further detail about the computation of m_{CO_2}). Note that, following (8), the limiting reactant is dolomite in the two mineralogical scenarios investigated in this work (Table 3). When the gas generation mechanism is activated, the reaction evolves over time until at least one primary phase is exhausted (see Section 1). We note that $\tilde{F}_{CO_2} \equiv 0$ when the mechanism is not activated (i.e., when $\tilde{Z}_{act}(t) = \emptyset$).

According to the conceptual model described above, at least one of the mineral phases involved in the CCR mechanism is expected to be exhausted at locations below the activation depth (i.e, for $Z > \tilde{Z}_{act}$) and the mineral phases equilibrium (1) leading to dissolved CO_2 is no longer

possible. We therefore assume that the dissolved amount of CO_2 is zero at all locations $Z > \tilde{Z}_{act}$ (see Electronic Annex I for additional details about the computational procedure).

3 Analysis of sources of uncertainty

Any model which aims at quantifying CO_2 generation in sedimentary basin is subject to considerable uncertainties. These are due to our incomplete knowledge of the processes involved and of the initial/boundary conditions together with the lack of information resulting from the large space-time scales, which are characteristic of the evolution of sedimentary systems. Upon following Neuman (2003), we distinguish in the following sections between modeling and parametric uncertainties. This work is keyed to the development and implementation of a methodology for the quantification of the uncertainty stemming from our incomplete knowledge of equilibrium reaction constants. In this section we frame this choice within the context of uncertainty quantification and discuss a variety of possible sources of uncertainty which may be relevant to our setting.

3.1 Model uncertainties

Investigation of complex settings in earth and environmental sciences typically relies on the formulation of a conceptual-mathematical model which is consistent with available information on the system investigated. Multiple and competing conceptual models can be formulated, according to diverse interpretations of the processes underlying the target scenario.

We list here key model uncertainties and the related assumptions associated with our setting.

- While we focus on the occurrence of reaction (8), other geochemical processes may take place simultaneously during basin compaction. Different competing models could therefore be formulated according to which reaction (8) occurs jointly with a set of diagenetic processes (e.g., dolomitization, albitization, illitization, cracking of biological matter and many others). All these processes can jointly contribute to CO_2

partial pressure and to increase/decrease or to the amount of CO_2 which can be found in the system. The selection of the geochemical processes which should be considered and the formulation of a related model is not a trivial task and constitutes a remarkable source of model uncertainty.

- The selection of the primary phases considered in the mineralogical assemblage is a key input to our methodology. This information is typically uncertain and various admissible hypotheses may be formulated, consistent with geological and sedimentological conceptual models and interpretations. Companion considerations hold on the assumed initial interstitial fluids composition (i.e., gas phase and brine). Our approach rests on the assumption that *i*) gaseous phase are CO_2 and H_2O , and *ii*) the initial pore-brine is pure water and the primary phases appearing in (8) are all available in the mineral composition. This is a simplification of the conditions encountered in real cases, but does not disable the proposed methodology.
- The spatial arrangement of the mineral composition may be affected by heterogeneity at all scales. In our conceptual model we assume a uniform spatial distribution of primary mineral phases throughout the carbonate-rich sedimentary layers. The spatial/temporal distribution of minerals could alternatively be described as a stochastic process, whose main features should possibly be characterized through real mineralogical samples of a specific sedimentary basin case study.

Quantification of the modeling uncertainties listed above may be performed through dedicated techniques (see, e.g., Neuman, 2003). While this task lies beyond the scope of the present work, we remark that these types of uncertainties should be carefully considered prior to applying the procedure outlined in Section 2 to the interpretation of observations from a real field site.

3.2 Parametric uncertainties

An admissible conceptual/mathematical model of a process commonly includes a number of parameters. These are in turn associated with a given level of uncertainty due to lack of information. This incomplete knowledge about parameter values can be quantified through, e.g. statistical characterization of available experimental data via parameter estimation techniques. In this work, we *a)* present a rigorous methodology to account for parametric uncertainty associated with mineral solubility equilibrium constants and *b)* propagate such uncertainty throughout our geochemical model of choice, which is aimed at representing CCR. While the need to account for these parameters is ubiquitous in geochemical models of environmental systems, a rigorous quantification of their uncertainty and its ensuing effects is often neglected. To sharply delineate the effect of this specific source of parametric uncertainty, we do not consider here other sources of parametric uncertainties such as: *a)* properties of the sedimentary rocks, i.e., density, permeability, thermal diffusivity and mechanical compressibility; *b)* boundary conditions of the compaction problem, i.e., heat flux at basin basement, and temporal dynamics of sea level evolution and sediment deposition rate; and *c)* other parameters of the geochemical model, including relative abundance of each mineral phase in the primary assemblage (for the given the qualitative composition of the mineralogy, which falls into the category of modeling uncertainties, as discussed in Section 3.1), molar volume change during the reaction (8), and activity and fugacity coefficients.

The influence of each set of parameters may be assessed through local and/or global sensitivity analysis techniques (e.g., Razavi and Gupta, 2015 and references therein), which we envision to explore in future works.

4 Results

This Section is devoted to a synthetic illustration of the results stemming from the implementation of the methodology proposed in Section 2.

4.1 Basin evolution

The results depicted in Fig. 3 are obtained through the numerical solution of the basin compaction model illustrated in Section 2.1. Fig. 3a depicts the space-time evolution of the vertical stratigraphic sequence of the basin (i.e., the system geo-history). The total basin thickness at present day is also shown. Fig. 3b-d respectively depict the space-time evolution of porosity, temperature and pressure with reference to the stratigraphy displayed in Fig. 3a. The black vertical lines identify the times when the sediment deposition rate (V_D) changes its value according to stepwise function described in Table 2 imposed at basin top.

4.2 Consistency of geochemical modeling results with field data

Here, we compare the results stemming from the application of our geochemical modeling approach against a set of field observations of CO_2 partial pressures reported by Coudrain-Ribstein et al. (1998). This comparison aims at assessing the robustness of our procedure and of the assumptions underlying the uncertainty quantification steps proposed in Section 2.2.1. We focus on the variation of $\log \tilde{K}_{R,T,P}$ and $\log \tilde{P}_{CO_2}$ as a function of temperature and pressure.

To this end, we perform a Monte Carlo sampling of the parameter space to obtain N realizations (here, we consider $N = 10^5$) of $\log \tilde{K}_{R,T,P}$ (6) as function of temperature and pressure. In the context of our comparison between field data and geochemical model outputs, we assume the following relationship between temperature and pressure (Smith and Ehrenberg, 1989; Cathles and Schoell, 2007)

$$P[bar] = 6(T[K] - 298) \quad (14)$$

Fig. 4a depicts the dependence on temperature of the mean, median, and 1st- and 99th-percentiles of the sample distribution of $\log \tilde{K}_{R,T,P}$. Here and in the following we denote a percentile (or quantile) of the distribution of a random variable $\tilde{\xi}$ as $p_w(\tilde{\xi})$. The latter is defined as the value below which

a percentage equal to W of observations of $\tilde{\zeta}$ falls. Note that the mean and the median coincide in Fig. 4a, $\log \tilde{K}_{R,T,P}$ being characterized by a symmetric sample distribution.

The Monte Carlo sample of $\log \tilde{P}_{CO_2}$ values can be obtained from $\log \tilde{K}_{R,T,P}$ through (3). Fig. 4b depicts percentiles $p_1(\log \tilde{P}_{CO_2})$, $p_{50}(\log \tilde{P}_{CO_2})$, and $p_{99}(\log \tilde{P}_{CO_2})$ as a function of temperature. These Monte Carlo - based results are juxtaposed in Fig. 4b to a set of available measurements of P_{CO_2} reported by Coudrain-Ribstein et al. (1998) for sedimentary formations. The consistency of the results provided by our geochemical model and the field data depicted in Fig. 4b is discussed in Section 5.1.

4.3 Quantitative assessment of CO_2 generation and CCR mechanism activation

We present here results associated with the way parametric uncertainty propagates to the outputs of the model described in Section 2.3, i.e., to the rate of generation of gaseous CO_2 and to the total dissolved CO_2 . Characterization of parameter uncertainty relies on the procedure described in Section 2.2.1. The results are related to the mineral compositions S_{dol} and S_{cal} (see Table 4) and are discussed in Section 5.2. All of the results presented are obtained upon relying on a sample of $N = 10^5$ Monte Carlo realizations.

Fig. 5 shows the vertical profiles of the percentiles of the partial pressure of CO_2 , $p_W(\log \tilde{P}_{CO_2} | C_{max})$, and of the ratio \tilde{R} as defined in (11), $p_W(\tilde{R})$ ($W = 1, 25, 50, 75, 99$), at two selected time levels ($t = 48, 0$ Ma) and for scenarios S_{dol} and S_{cal} . To complement this result, Fig. 6 provides a comparison of the sample *cdf* (cumulative distribution function) of \tilde{R} (11) at $Z = 8$ km for scenarios S_{dol} and S_{cal} . Note that at $t = 0$ the top layer ($0 < Z < 1.4$ km) of the basin is formed by mudrocks (see Fig. 3a). Therefore, we set $P_{CO_2} = 0$ at these locations (see Fig. 5b and d), as we assume CCR happens exclusively in carbonates layers.

The probability of activation $G_A(t)$ can then be as the sample probability (relative frequency) of observing at least one point in the domain for which $\tilde{R} \geq 1$, i.e., the generation of CO_2 as a separate

phase through CCR is activated at time t . The procedure to compute G_A is exemplified in Fig. 6, where the value $R = 1$ is identified by a vertical red line, which represents the conditions at which the CO_2 generation as a separate gas phase is activated (see Section 2.3). The *cdfs* associated with the two diverse mineral compositions intercept the threshold line corresponding to $R = 1$ (i.e., the conditions at which the CO_2 generation as a separate gas phase is activated) at different points, i.e., for $R = 1$ the *cdf* attains a value equal to 0.55 and 0.85, respectively for S_{dol} and S_{cal} , indicating a different probability of activation in the two scenarios. Fig. 7 depicts the temporal evolution of $G_A(t)$ for S_{dol} and S_{cal} across the overall basin history.

Our procedure allows identifying not only the probability of activation at given time but also to estimate the location of the CO_2 sources through (12). Fig. 8 depicts the sample probability (relative frequency) $f_{Zact,t}$ that the activation of gaseous CO_2 generation takes place at location \tilde{Z}_{act} at time t . In particular Fig. 8a displays $f_{Zact,10}$, i.e., $f_{Zact,t}$ for $t = 10$ Ma, where the domain is comprised between the sea bottom (at 106 m) and 7.6 Km. We note that this relative frequency is computed upon considering the complete set of Monte Carlo realizations, including those for which $\tilde{Z}_{act} = \emptyset$ according to (12). Thus, the function $f_{Zact,t}$ integrates to the corresponding value of G_A at time t i.e.

$$\int_{\Omega_Z(t)} f_{Zact,t} dZ = G_A(t) \quad (15)$$

For example, the integral (15) evaluated at $t = 10$ Ma for scenario S_{dol} is equal to 0.30, which corresponds to the value of $G_A(t=10 \text{ Ma})$ for the corresponding scenario reported in Fig. 7. Fig. 8b-c depict the temporal dynamics of the relative frequency $f_{Zact,t}$ for scenarios S_{dol} and S_{cal} . As anticipated by the temporal variation of $G_A(t)$ in Fig. 7 the nonzero values are obtained for $t < 50$ Ma in both scenarios. The generation of gaseous CO_2 takes place at $\tilde{Z}_{act} > 4.8$ km in the considered example for both mineral composition scenarios.

Figure 9-10 provide the probabilistic quantification of the generated CO_2 in terms of (i) flux of gaseous CO_2 generated as a result of the CCR process. \tilde{F}_{CO_2} , as defined in (13), and (ii) concentration of dissolved CO_2 $\tilde{C}_{CO_2(aq)} \Big| \left(C_{max}, \tilde{Z}_{act} \right)$. Fig. 9a depicts the relative frequency $f_{F,t}$ associated with $\log \tilde{F}_{CO_2}$ at time t for the overall basin history of scenario S_{dol}. Corresponding results for S_{cal} are depicted in Fig. 9b. We set here $L = 1 \text{ m}^2$ in (13) so that the reported values of \tilde{F}_{CO_2} are per unit (planar) area of the sedimentary basin. For completeness, Fig. 9a-b include the information (black solid curve) corresponding to the frequency of activation $G_A(t)$. Note that $G_A(t) \equiv 0$ for $t \in] 45 \text{ Ma}, 135 \text{ Ma}]$, thus implying that $\tilde{F}_{CO_2} \equiv 0$ across all Monte Carlo realizations for these simulation times. Indeed, $f_{F,t} = 0$ for all non-zero values of \tilde{F}_{CO_2} for $t \in] 45 \text{ Ma}, 135 \text{ Ma}]$. Fig. 9c depicts the sample *cdfs* of \tilde{F}_{CO_2} associated with the two time levels identified by the red dashed vertical lines in Fig. 9a, i.e., $t = 20$, and 0 Ma .

Figure 10 reports the distribution along the basin depth of the relative frequency associated with the log-concentration $\log \tilde{C}_{CO_2(aq)} \Big| \left(C_{max}, \tilde{Z}_{act} \right)$ (denoted as $f_{C,Z}$ in Fig. 10a-b). Introducing here $f_{C,Z}(0)$ to denote the relative frequency associated with $\tilde{C}_{CO_2(aq)} \Big| \left(C_{max}, \tilde{Z}_{act} \right) = 0$, Fig. 10c, d) display the variation of $f_{C,Z}(0)$ with Z for the two mineral compositions S_{dol} and S_{cal}, respectively.

5 Discussion

This Section is devoted to the discussion and interpretation of the results illustrated in Section 4. We focus in particular on the key results obtained in terms of the probabilistic assessment of CO_2 generation through CCR.

5.1 Geochemical modeling results

With reference to Fig. 4a, we observe that all percentiles associated with $\log \tilde{K}_{R,T,P}$ tend to increase with temperature and pressure. Fig. 4a shows that a negligible probability is associated with positive values of $\log \tilde{K}_{R,T,P}$ when $T < 50$ °C, i.e. the equilibrium (8) favors primary phases over secondary phases. Otherwise, our results indicate that a probability very close to 1 is associated with values of $\log \tilde{K}_{R,T,P} > 0$ for $T > 100$ °C. This finding is consistent with the results of Smith and Ehrenberg (1989) who suggest that CO_2 formation is typically favored above 100-120°C as a consequence of carbonate phase consumption.

Fig. 4b, shows that the partial pressure of CO_2 tends to increase with temperature as a direct consequence of the trend of $\log \tilde{K}_{R,T,P}$ in Fig. 4a. The median value of $\log \tilde{P}_{CO_2}$, $p_{50}(\log \tilde{P}_{CO_2})$ is consistent with field observations (e.g., Texas, Norway and Thailand basins in Fig. 4b) for temperature values higher than 100 °C. Almost all of the field data reported by Coudrain-Ribstein et al. (1998) for this temperature range fall between $p_1(\log \tilde{P}_{CO_2})$ and $p_{99}(\log \tilde{P}_{CO_2})$, with the exception of a very limited number of points. Otherwise, the majority of the field data (mainly associated with Alberta, Paris, Arkansans and Medison basins in Fig. 4b) falls outside the range identified by $p_1(\log \tilde{P}_{CO_2})$ and $p_{99}(\log \tilde{P}_{CO_2})$ for $T < 100$ °C. The median value of $\log \tilde{P}_{CO_2}$ resulting from our simulations tends to overestimate the field data in this temperature range. Giggenbach (1981) suggests that dilution of aqueous CO_2 in the system at shallow depth (corresponding to low temperature) can happen due to mixing of fresh and cold water (i.e., from meteoric precipitations) with groundwater. Moreover, Coudrain- Ribstein et al. (1998) observe that complex minerals such as illite or competing geochemical processes can play a relevant role at low temperature levels. The discussion of the consistency of the data with possible alternatives of physical and conceptual models as the ones suggested above is beyond the scope of the present work as previously explained in

Section 3.1. Here, we can highlight that our procedure leads to results which are consistent with the degree of variability of P_{CO_2} values observed in real systems at temperatures $T > 100$ °C.

5.2 CO_2 generation and CCR mechanism activation

We start our discussion by considering the characterization of \tilde{P}_{CO_2} as function of depth. All values of $p_W(\log \tilde{P}_{CO_2} | C_{max})$ display a monotonic increase with depth (Fig. 5a-b) at the considered times and for both mineralogical composition scenarios. This behavior is consistent with the observation that (i) temperature and pressure increase with depth at all times (see Fig. 3c and d); and (ii) the equilibrium constant $\log \tilde{K}_{R,T,P}$ increases with temperature and pressure (see Fig. 4a), i.e., formation of CO_2 is favored by the increase of temperature and pressure. Partial pressure of CO_2 is computed only in those layers within which there is a mineral composition compatible with the CCR process, labeled as carbonate layers in Figure 3. The total basin thickness at $t = 48$ Ma is approximately equal to 5.5 km, the basin being completely constituted by carbonates rocks (see Fig. 4a). Thus, we find $\tilde{P}_{CO_2} | C_{max} > 0$ across the whole computational domain (Fig. 5a). The impact of the limiting reactant associated with the two mineral composition scenarios is negligible at this time level and no significant differences are detected between values of $p_W(\log \tilde{P}_{CO_2} | C_{max})$ computed for scenarios S_{cal} and S_{dol} . We can then conclude that the dissolved CO_2 concentration values rendered by the geochemical model at this time do not exceed the value of the maximum admissible concentration associated with either S_{dol} or S_{cal} . Otherwise, the mineral composition at $t = 0$ Ma influences the statistical characterization of $\log \tilde{P}_{CO_2} | C_{max}$ at large depths ($Z > 6$ km). We observe that $p_W(\log \tilde{P}_{CO_2} | C_{max})$ displays a different trend for depths larger than 6 km, according to the mineralogical composition considered. Fig. 6b suggests that the effect of limiting reactant affects all probability levels, i.e., $p_W(\log \tilde{P}_{CO_2} | C_{max}(S_{dol})) > p_W(\log \tilde{P}_{CO_2} | C_{max}(S_{cal}))$ for all considered values

of W even as the value of C_{max} (quantifying the effect of limiting reactant) is a deterministically imposed upper boundary (see the Electronic Annex III for additional details).

We then discuss the results obtained in terms of the activation of the generation of gaseous CO_2 . Values of \tilde{R} associated with all of the considered percentiles $p_l(\tilde{R})$ increase with depth for both time levels considered (see Fig. 5c-d). This result indicates that the sum of gas partial pressures (\tilde{P}_{CO_2} and P_{H_2O}) tends to increase with depth at a faster rate than does the fluid pressure P . The difference $p_{99}(\tilde{R}) - p_1(\tilde{R})$ markedly increases with depth, suggesting that the level of uncertainty associated with \tilde{P}_{CO_2} tends to increase with temperature and pressure. Consistent with Fig. 5b, the mineral composition scenario influences these results only for $Z > 6$ km. Fig. 6 presents the comparison of the sample *cdfs* (cumulative distribution functions) of \tilde{R} (11) at $Z = 8$ km for scenarios S_{dol} and S_{cal} . We observe that the relative proportions among the different minerals constituting the sediments influences the statistical distribution of \tilde{R} and, consequently, the probability of generation of gaseous CO_2 .

The value of the sample probability of generation of gaseous CO_2 $G_A(t)$ increases with time (Fig. 7) and attains its highest value for the final simulation time ($t = 0$ Ma). It is possible to distinguish three stages according to the time evolution of $G_A(t)$: (i) for $t \in] 45 \text{ Ma}, 135 \text{ Ma}]$, where $G \equiv 0$; (ii) for $t \in] 20 \text{ Ma}, 45 \text{ Ma}]$, where $0 < G < 0.2$, with comparable values for S_{dol} and S_{cal} ; and (iii) for $t \in] 0 \text{ Ma}, 20 \text{ Ma}]$, where G_A continuously increases, with a trend which varies according to the mineralogical scenario. It can be noted that the probability of activation grows slower in time for scenario S_{cal} than for S_{dol} .

Our results suggest that the temperature range associated with locations where the activation of the process is possible, i.e., at which $f_{Zact,\tau} > 0$, is comprised between 200 and 300 °C (compare Fig. 8b-c with Fig. 4c). This information can be highly valuable, e.g., to assess the prior probability of CCR being a key source of CO_2 in natural systems (e.g., Jarvie and Jarvie, 2007). Cathles and

Schoell (2007) predict an activation temperature of 330°C through a deterministic approach similar to the one presented in Section 2 and a simple time-independent P - T relationship. Our results suggest that the generation of gaseous CO_2 by CCR might take place also at lower temperatures when the parametric uncertainty related to the geochemical model are considered.

With reference to the results depicted in Fig. 9 and related to the probabilistic analysis of \tilde{F}_{CO_2} , we note that nonzero (positive) values of the latter can be found only if the CCR mechanism is active at a given time, i.e., if $\tilde{Z}_{act}(t) \neq \emptyset$, \tilde{F}_{CO_2} being equal to zero otherwise. The contour lines describing $f_{F,t}$ in Fig. 9a-b are qualitatively very similar. However, we observe a remarkable quantitative difference between the two scenarios analyzed: non-zero values of \tilde{F}_{CO_2} range between 12 and 31 ton/Ma in scenario S_{dol} , while these are comprised between 1.0 and 2.5 ton/Ma for S_{cal} . This result can be ascribed to the effect of the diverse fractions of dolomite characterizing S_{dol} and S_{cal} and acting as the limiting reactant. The *cdfs* reported in Fig. 9c indicate that the nonzero values of \tilde{F}_{CO_2} display a modest variability for a given time level. This suggests that, even as the location of the source is characterized by remarkable variability across the Monte Carlo sample (see Fig. 8), porosity and sediment velocity which contribute to \tilde{F}_{CO_2} according to (13) display modest variability along the region of vertical domain where $f_{Zact,t} > 0$. Our results also show that the nonzero values of \tilde{F}_{CO_2} observed at $t = 20$ Ma in the Monte Carlo sample are fewer than those obtained at $t = 0$ Ma. Note that the non-zero values of \tilde{F}_{CO_2} detected at $t = 20$ Ma are larger than their non-zero counterparts arising at $t=0$ Ma. For those realizations within which the generation of gaseous CO_2 is activated, we obtain a CO_2 generation rate of about 27 and 18 ton/Ma, respectively at $t = 20$, and 0 Ma. This difference is a consequence of the diverse values of the sediment burial velocity ($V_{SED}(\tilde{Z}_{act}, t)$ in (13)) at the location where gaseous CO_2 is generated. We exclude that porosity can play a relevant role in the different \tilde{F}_{CO_2} values obtained at $t = 0$ and 20 Ma as it is almost constant (approximately equal to 0.1) for $Z > 4$ km, where the CO_2 source is located (see Fig. 3c).

We conclude our discussion by considering the distribution of $\log \tilde{C}_{CO_2(aq)} \left| \left(C_{max}, \tilde{Z}_{act} \right) \right.$ (Eq.I.23 in the Electronic Annex I) depicted in Fig. 10. We recall that quantity $f_{C,Z}(0)$ denotes the relative frequency associated with $\tilde{C}_{CO_2(aq)} \left| \left(C_{max}, \tilde{Z}_{act} \right) = 0 \right.$. Fig. 10c, d) respectively depict the dependence of $f_{C,Z}(0)$ on Z for S_{dol} and S_{cal} . Note that, according to our conceptual model, $\tilde{C}_{CO_2(aq)} \left| \left(C_{max}, \tilde{Z}_{act} \right) = 0 \right.$ at all locations where mudstone layers are found and below the depth Z_{act} . As such, we find $f_{C,Z}(0) = 1$ at $0 < Z < 1.4$ km. We observe that $f_{C,Z}(0) \equiv 0$ at $1.4 < Z < 4.5$ km, suggesting that the concentration of dissolved CO_2 attains non-zero values across the complete Monte Carlo set. Finally, the relative frequency $f_{C,Z}(0)$ attains values higher than zero and lower than one and increases with depth for $Z > 4.5$ km. This finding is consistent with results of Fig. 8, showing that (i) $Z = 4.5$ km is the shallowest location at which the activation of the CCR mechanism is possible at $t = 0$ Ma and (ii) the probability to observe vanishing CO_2 concentrations at a given location increases with the relative frequency that the depth of such a location is larger than that corresponding to Z_{act} .

Calculated values for concentration of dissolved CO_2 display negligible dependence on mineral composition scenario, in contrast with \tilde{F}_{CO_2} (Fig. 9). The only impact of the mineral composition scenario on $f_{C,Z}$ is due to the upper bound C_{max} imposed by the availability of reactants which leads to an increase of the relative frequency $f_{C,Z}$ of values $\tilde{C}_{CO_2(aq)} \left| \left(C_{max}, \tilde{Z}_{act} \right) = C_{max} \right.$ at large depths within S_{cal} (see Fig. 10b). This behavior follows from the observation that the extent of the region where the reaction can occur is limited by the available dolomite volume fraction in S_{cal} (see Fig. 10d).

6 Conclusions

We present a methodology conducive to a probabilistic assessment of the amount of CO_2 generated in sedimentary basins as consequence of the interaction between carbonate and clay

minerals in the presence of pore-water. Our modeling strategy rests on the quantification of the uncertainty of chemical equilibrium parameters related to mineral solubility and the way it propagates to key model outputs. Application of the proposed workflow leads to a probabilistic assessment of: (i) the evolution of CO_2 partial pressure and dissolved CO_2 as a function of depth and time along the basin burial history; (ii) the location of the source where gaseous CO_2 is released from the sediments; (iii) the amount of gaseous CO_2 released per unit time.

We illustrate our approach upon relying on a realistic basin compaction history meaning that temperature-pressure-porosity combinations are compatible with realistic fields. Our work provides a first attempt to quantify CO_2 generation by CCR at geological scales with the explicit inclusion of a probabilistic assessment of the uncertainty stemming from the incomplete knowledge of mineral solubility and phase equilibrium constants at high temperatures. Due to its flexibility, we envision that the framework proposed here can be readily extended to include the uncertainty related to the basin pressure and temperature dynamics. We envision that the proposed model may be extended in future works to include other sources of model uncertainty, such as those associated with pore-water chemistry (e.g., salinity).

Our uncertainty quantification is based on data of mineral solubility and phase equilibrium constants available at laboratory scales. We verify that the procedure we employ to characterize parametric uncertainty of the geochemical model leads to results which are consistent with field observations of CO_2 partial pressure in sedimentary formations reported in the literature.

Our study shows that the partial pressure of CO_2 displays a monotonic and increasing trend with depth. This suggests that the increase of temperature taking place during a basin burial history favors the progressive generation of CO_2 at the expense of carbonate mineral phases. CO_2 is generated as a separate phase only under specific conditions which depend on temperature and pressure distributions. The probability that these conditions are encountered tends to increase with time and attains its largest value (around 0.45 in the setting we analyze) at the end of the simulation period, which represent the present day. In our example we find that generation of CO_2 through CCR can

become effective at temperatures comprised between 200 and 300 °C. These specific results are conditional to the given compaction history of the basin and of the geochemical model structure selected in this study are therefore not amenable to direct transferability to diverse geological settings.

Mineral compositions associated with sediments largely affect the flux of generated CO_2 . In the case we examine, the key driver is the amount of dolomite associated with the sediments and representing the source of CO_2 . In our illustrative example, the impact of model parameter uncertainty is stronger on the activation depth than on the CO_2 generation rate. As a consequence, our findings suggest that reliable estimates of CO_2 migration scenarios should rely on accurate characterization of mineral composition as well as geochemical model parameters.

7 Acknowledgments

We acknowledge financial support by Eni spa.

References

- Allis R., Chidsey T., Gwynn W., Morgan C., White S., Adams M. & Moore J. (2001). Natural CO_2 reservoirs on the colorado plateau and southern rocky mountains: Candidates for CO_2 sequestration. *Proceedings of the First National Conference on Carbon Sequestration*, 14-17.
- Anderson G. M. (2009). *Thermodynamics of natural systems* Cambridge University Press.
- Arnórsson S. (1986). Chemistry of gases associated with geothermal activity and volcanism in iceland: A review. *J. Geophys. Res. B: Solid Earth*, **91(B12)**, 12261-12268.
- Ballentine C. J., Schoell M., Coleman D. & Cai B. A. (2001). 300-myr-old magmatic CO_2 in natural gas reservoirs of the west texas permian basin. *Nature*, **409(6818)**, 327-331.

- Battistelli A., Berry P., Bonduà S., Bortolotti V., Consonni A., Cormio C. Geloni C. & Vasini E. M. (2016) Thermodynamics-related processes during the migration of acid gases and methane in deep sedimentary formations. *GREENH GASES*.
- Bergaya F. & Lagaly G. (2013). General Introduction: Clays, Clay Minerals, and Clay Science. *Handbook of Clay Science*, 1, 1.
- Bianchi Jannetti E., Dror I., Riva M., Guadagnini A. & Berkowiz B. (2012). Estimation of Single-Metal and Competitive Sorption Isotherms through Maximum Likelihood and Model Quality Criteria. *Soil Sci. Soc. Am. J.* **76**, 1229–1245.
- Blanc P., Lassin A., Piantone P., Azaroual M., Jacquemet N., Fabbri A., & Gaucher E. C. (2012). Thermoddem: A geochemical database focused on low temperature water/rock interactions and waste materials. *Appl. Geochem.*, **27(10)**, 2107-2116.
- Blanc P., Vieillard P., Gailhanou H., & Gaboreau S. (2013). Thermodynamics of clay minerals. *Handbook of Clay Science*, 6, 173.
- Blanc P., Vieillard P., Gailhanou H., Gaboreau S., Gaucher É., Fialips C. I., Madé B. & Giffaut E. (2015). A generalized model for predicting the thermodynamic properties of clay minerals. *Am. J. S.*, **315(8)**, 734-780.
- Broadhead R. F., Mansell M. & Jones G. (2009). Carbon Dioxide in New Mexico: Geologic Distribution of Natural Occurrences. *New Mexico Bureau of Geology and Mineral Resources Open-file Report 514*.
- Cai C., Hu W., & Worden R. H. (2001). Thermochemical sulphate reduction in Cambro–Ordovician carbonates in central Tarim. *Mar. Pet. Geol.*, **18(6)**, 729-741.

- Cathles L. & Schoell M. (2007). Modeling CO₂ generation, migration, and titration in sedimentary basins. *Geofluids*, **7(4)**, 441-450.
- Chiodini G., Baldini A., Barberi F., Carapezza M., Cardellini C., Frondini F., Granieri D. & Ranaldi M. (2007). Carbon dioxide degassing at Lateral caldera (Italy): Evidence of geothermal reservoir and evaluation of its potential energy. *J. Geophys. Res. B: Solid Earth*, **112(B12)**.
- Chiodini G., Frondini F., Cardellini C., Parello F. & Peruzzi L. (2000). Rate of diffuse carbon dioxide earth degassing estimated from carbon balance of regional aquifers: The case of central apennine, Italy. *J. Geophys. Res. B: Solid Earth*, **105(B4)**, 8423-8434.
- Clayton J., Spencer C., Koncz I. & Szalay A. (1990). Origin and migration of hydrocarbon gases and carbon dioxide, Bekes basin, southeastern Hungary. *Org. Geochem.*, **15(3)**, 233-247.
- Colombo I., Porta G. M., Ruffo P., Guadagnini A. (2016). Assessment of overpressure buildup through inverse modeling of compaction processes in sedimentary basins. *Hydrol. J. (accepted)*.
- Cooper B., Raven M. & Samuel L. (1997). Origin and geological controls on subsurface CO₂ distribution with examples from western Indonesia. *Proceedings of an International Conference on Petroleum Systems of SE Asia and Australasia*, 877-892
- Coudrain-Ribstein A. & Gouze P. (1993). Quantitative study of geochemical processes in the dogger aquifer, paris basin, france. *App. Geochem.*, **8(5)**, 495-506.
- Coudrain-Ribstein A., Gouze P. & de Marsily G. (1998). Temperature-carbon dioxide partial pressure trends in confined aquifers. *Chem. Geol.*, **145(1)**, 73-89.
- Delany J. & Lundeen S. (1990). The LLNL thermochemical database. Lawrence Livermore National Laboratory Report UCRL-21658.

- Dubacq B., Bickle M. J., Wigley M., Kampman N., Ballentine C. J. & Lollar B. S. (2012). Noble gas and carbon isotopic evidence for CO₂-driven silicate dissolution in a recent natural CO₂ field. *Earth Planet. Sci. Lett.*, **341**, 10-19.
- Farmer R. (1965). Genesis of subsurface carbon dioxide. *Fluids in Subsurface Environments, A Symposium*.
- Fischer M., Botz R., Schmidt M., Rockenbach K., Garbe-Schönberg D., Glodny J., Gerling R., Littke R. (2006). Origins of CO₂ in permian carbonate reservoir rocks (zechstein, Ca₂) of the NW-german basin (lower saxony). *Chem. Geol.*, **227**(3), 184-213.
- Formaggia L., Guadagnini A., Imperiali I., Lever V., Porta G., Riva M., Scotti A., Tamellini L. (2013). Global sensitivity analysis through polynomial chaos expansion of a basin-scale geochemical compaction model. *Comput. Geosci.*, **17**(1), 25-42.
- Giggenbach W. F. (1978). The isotopic composition of waters from the el tatio geothermal field, northern chile. *Geochim. Cosmochim. Acta*, **42**(7), 979-988.
- Giggenbach W. F. (1980). Geothermal gas equilibria. *Geochim. Cosmochim. Acta*, **44**(12), 2021-2032.
- Giggenbach W. F. (1981). Geothermal mineral equilibria. *Geochim. Cosmochim. Acta*, **45**(3), 393-410.
- Giggenbach W. F. (1984). Mass transfer in hydrothermal alteration systems—a conceptual approach. *Geochim. Cosmochim. Acta*, **48**(12), 2693-2711.
- Goldsmith J. R. (1980). Thermal stability of dolomite at high temperatures and pressures. *J. Geophys. Res. B: Solid Earth*, **85**(B12), 6949-6954.

- Higgs K. E., Funnell R. H. & Reyes A. G. (2013). Changes in reservoir heterogeneity and quality as a response to high partial pressures of CO₂ in a gas reservoir, New Zealand. *Mar. Pet. Geol.*, **48**, 293-322.
- Huang W. & Longo J. (1994). Experimental studies of silicate-carbonate reactions—I. applications to diagenesis. *App. Geochem.*, **9(5)**, 501-522.
- Hutcheon I. (1990). Clay carbonate reactions in the venture area, Scotian shelf, Nova Scotia, Canada. *Geo. Soc. S. P.*, **2**, 199-212.
- Hutcheon I. & Abercrombie H. (1990). Carbon dioxide in clastic rocks and silicate hydrolysis. *Geology*, **18(6)**, 541-544.
- Hutcheon I., Abercrombie H. J. & Krouse H. (1990). Inorganic origin of carbon dioxide during low temperature thermal recovery of bitumen: Chemical and isotopic evidence. *Geochim. Cosmochim. Acta*, **54(1)**, 165-171.
- Hutcheon I., Abercrombie H. J., Putnam P., Gardner R. & Krouse H. R. (1989). Diagenesis and sedimentology of the clearwater formation at tucker lake. *B. Can. Petrol. Geol.*, **37(1)**, 83-97.
- Hutcheon I., Oldershaw A. & Ghent E. D. (1980). Diagenesis of cretaceous sandstones of the kootenay formation at elk valley (southeastern british columbia) and mt allan (southwestern alberta). *Geochim. Cosmochim. Acta*, **44(10)**, 1425-1435.
- Hutcheon I., Shevalier M., & Abercrombie H. J. (1993). pH buffering by metastable mineral-fluid equilibria and evolution of carbon dioxide fugacity during burial diagenesis. *Geochim. Cosmochim. Acta*, **57(5)**, 1017-1027.
- Imbus S. W., Katz B. J. & Urwongse T. (1998). Predicting CO₂ occurrence on a regional scale: Southeast Asia example. *Org. Geochem.*, **29(1)**, 325-345.

- Jarvie D. M. & Jarvie B. M. (2007). Thermal decomposition of various carbonates: kinetic results and geological temperatures of conversion. *23th international meeting on Organic Geochemistry (IMOG), Torquay, UK, 9-14 September 2007.*
- Johnson J. W., Oelkers E. H. & Helgeson H. C. (1992). SUPCRT92: A software package for calculating the standard molal thermodynamic properties of minerals, gases, aqueous species, and reactions from 1 to 5000 bar and 0 to 1000 C. *Comput. Geosci.*, **18**(7), 899-947.
- Kharaka Y. K., Gunter W. D., Aggarwal P. K., Perkins E. H. & De Braal J. D. (1988). SOLMINEQ. 88: A computer program for geochemical modeling of water-rock interactions. *US Geological Survey Water-Resources Investigation Report*, **88**, 4227.
- Kotarba M. J. & Nagao K. (2008). Composition and origin of natural gases accumulated in the polish and ukrainian parts of the carpathian region: Gaseous hydrocarbons, noble gases, carbon dioxide and nitrogen. *Chem. Geol.*, **255**(3), 426-438.
- Li M., Wang T., Liu J., Lu H., Wu W. & Gao L. (2008). Occurrence and origin of carbon dioxide in the fushan depression, beibuwan basin, south china sea. *Mar. Pet. Geol.*, **25**(6), 500-513.
- Maier C. G. & Kelley K. (1932). An equation for the representation of high-temperature heat content data1. *J. Am. Chem. Soc.*, **54**(8), 3243-3246.
- Mayo A. L. & Muller A. B. (1997). Low temperature diagenetic–metamorphic and magmatic contributions of external CO₂ gas to a shallow ground water system. *J. Hydrol.*, **194**(1), 286-304.
- Metz B., Davidson O., De Coninck H., Loos M., & Meyer L. (2005). IPCC, 2005: IPCC special report on carbon dioxide capture and storage. prepared by working group III of the

intergovernmental panel on climate change. *Cambridge, United Kingdom and New York, NY, USA*, 442.

Millero F. J. (1982). The effect of pressure on the solubility of minerals in water and seawater. *Geochim. Cosmochim. Acta*, **46(1)**, 11-22.

Neuman S. P. (2003). Maximum likelihood Bayesian averaging of uncertain model predictions. *Stoch. Environ. Res. Risk Ass.*, **17**, 291-305.

Parkhurst D. L. & Appelo C. (2013). Description of input and examples for PHREEQC version 3—a computer program for speciation, batch-reaction, one-dimensional transport, and inverse geochemical calculations. *US Geological Survey Techniques and Methods, Book, 6*, 497.

Peterson S. R., Hostetler C. J., Deutsch W. J. & Cowan C. E. (1987). *MINTEQ user's manual* (No. NUREG/CR-4808; PNL-6106). Pacific Northwest Lab., Richland, WA (USA); Nuclear Regulatory Commission, Washington, DC (USA). Div. of Waste Management.

Plummer L. N. & Busenberg E. (1982). The solubilities of calcite, aragonite and vaterite in CO₂-H₂O solutions between 0 and 90 C, and an evaluation of the aqueous model for the system CaCO₃-CO₂-H₂O. *Geochim. Cosmochim. Acta*, **46(6)**, 1011-1040.

Porta G., Tamellini L., Lever V. & Riva M. (2014). Inverse modeling of geochemical and mechanical compaction in sedimentary basins through polynomial chaos expansion. *Water Resour. Res.*, **50(12)**, 9414-9431.

Razavi S. & Gupta H. V. (2015). What do we mean by sensitivity analysis? the need for comprehensive characterization of “global” sensitivity in earth and environmental systems models. *Water Resour. Res.*, **51(5)**, 3070-3092.

- Riva M., Guadagnini A. & Dell'Oca A. (2015). Probabilistic assessment of seawater intrusion under multiple sources of uncertainty. *Adv. Water Resour.*, **75**, 93-104.
- Saltelli A., Ratto M., Andres T., Campolongo F., Cariboni J., Gatelli D., Saisana M. , Tarantola S. (2008). *Global sensitivity analysis: The primer* John Wiley & Sons.
- Smith J. & Ehrenberg S. (1989). Correlation of carbon dioxide abundance with temperature in clastic hydrocarbon reservoirs: Relationship to inorganic chemical equilibrium. *Mar. Pet. Geol.*, **6(2)**, 129-135.
- Sobol I. M. (2001). Global sensitivity indices for nonlinear mathematical models and their Monte Carlo estimates. *Mat. Comput. Simul.*, **55(1)**, 271-280.
- Span R. & Wagner W. (1996). A new equation of state for carbon dioxide covering the fluid region from the triple-point temperature to 1100 K at pressures up to 800 MPa. *J. Phys. Chem. Ref. Data*, **25(6)**, 1509-1596.
- Stumm W. & Morgan J. (1996). Aquatic chemistry: Chemical equilibria and rates in natural waters. *John Wiley & Sons: New York*, 1040.
- Spycher N., Pruess K., & Ennis-King J. (2003). CO₂-H₂O mixtures in the geological sequestration of CO₂. *Geochim. Cosmochim. Acta* **67**,3015.
- Ueda A., Kato K., Ohsumi T., Yajima T., Ito H., Kaieda H., Metcalfe R. & Takase H. (2005). Experimental studies of CO₂-rock interaction at elevated temperatures under hydrothermal conditions. *Geochem. J.*, **39(5)**, 417-425.
- van Berk W., Schulz H. & Fu Y. (2009). Hydrogeochemical modelling of CO₂ equilibria and mass transfer induced by organic–inorganic interactions in siliciclastic petroleum reservoirs. *Geofluids*, **9(4)**, 253-262.

- van Berk W., Schulz H. & Fu Y. (2013). Controls on CO₂ fate and behavior in the gullfaks oil field (norway): How hydrogeochemical modeling can help decipher organic-inorganic interactions. *AAPG Bull.*, **97(12)**, 2233-2255.
- Wycherley H., Fleet A. & Shaw H. (1999). Some observations on the origins of large volumes of carbon dioxide accumulations in sedimentary basins. *Mar. Pet. Geol.*, **16(6)**, 489-494.
- Xu T. & Pruess K. (2001). On fluid flow and mineral alteration in fractured caprock of magmatic hydrothermal systems. *J. Geophys. Res. B: Solid Earth*, **106(B2)**, 2121-2138.
- Yaalon D. H. (1962). Mineral composition of the average shale. *Clay Miner.*, **5(27)**, 31-36.
- Zhang S., FitzGerald J. D. & Cox S. F. (2000). Reaction-enhanced permeability during decarbonation of calcite quartz → wollastonite carbon dioxide. *Geology*, **28(10)**, 911-914.